

Fabrication and full characterization of state-of-the-art quantum dot luminescent solar concentrators

Jana Bomm^{a,*}, Andreas Büchtemann^a, Amanda J. Chatten^b, Rahul Bose^b, Daniel J. Farrell^b, Ngai L.A. Chan^b, Ye Xiao^b, Lenneke H. Slooff^c, Toby Meyer^d, Andreas Meyer^d, Wilfried G.J.H.M. van Sark^e, Rolf Koole^f

^a Fraunhofer Institute for Applied Polymer Research (IAP), Geiselbergstraße 69, 14476 Potsdam, Germany

^b Department of Physics, Imperial College London, South Kensington Campus, London SW7 2AZ, UK

^c ECN Solar Energy, P.O. Box 1, 1755 ZG Petten, The Netherlands

^d Solaronix SA, Rue de l'Ouverture 129, 1170 Aubonne, Switzerland

^e Science, Technology and Society, Copernicus Institute of Sustainable Development and Innovation, Utrecht University, Heidelberglaan 2, 3584 CS Utrecht, The Netherlands

^f Chemistry of Condensed Matter, Debye Institute for Nanomaterials Science, Utrecht University, Princetonplein 1, 3584 CC Utrecht, The Netherlands

ARTICLE INFO

Article history:

Received 27 October 2010

Received in revised form

23 February 2011

Accepted 25 February 2011

Available online 25 March 2011

Keywords:

Quantum dots

Luminescent solar concentrators

Nanocomposites

Quantum yield

Solar cells

Ray-trace model

ABSTRACT

The fabrication and full characterization of luminescent solar concentrators (LSCs) comprising CdSe core/multishell quantum dots (QDs) is reported. TEM analysis shows that the QDs are well dispersed in the acrylic medium while maintaining a high quantum yield of 45%, resulting in highly transparent and luminescent polymer plates. A detailed optical analysis of the QD-LSCs including absorption, emission, and time-resolved fluorescence measurements is presented. Both silicon and GaAs solar cells attached to the side of the QD-LSCs are used to measure the external quantum efficiency and power conversion efficiency (2.8%) of the devices. Stability tests show only a minor decrease of 4% in photocurrent upon an equivalent of three months outdoor illumination. The optical data are used as input for a ray-trace model that is shown to describe the properties of the QD-LSCs well. The model was then used to extrapolate the properties of the small test devices to predict the power conversion efficiency of a $50 \times 50 \text{ cm}^2$ module with a variety of different solar cells. The work described here gives a detailed insight into the promise of QD-based LSCs.

© 2011 Elsevier B.V. All rights reserved.

1. Introduction

The concept of a luminescent solar concentrator (LSC) for photovoltaic applications was proposed in the late 1970s by Goetzberger and Greubel [2] and Weber and Lambe [1]. LSCs traditionally consist of a planar sheet of transparent polymer or glass, doped with luminescent organic dyes. The incident sunlight is absorbed by the luminescent dye and the red-shifted re-emitted light is wave guided by total internal reflection to the small edges, where it is coupled into a photovoltaic cell (PVC) and converted into electricity (Fig. 1a). For a dye doped polymer sheet with a refractive index of approximately 1.5, about 75% of the re-emitted light can be trapped in the LSC [3]. Loss mechanisms for such a device include emission of photons within the escape-cone, matrix absorption, and a luminescence quantum yield (QY) of the dye less than 100%. Re-absorption of emitted photons by the dye is a major loss mechanism in LSCs, because it introduces a

further chance for emission within the escape-cone or non-radiative recombination. In order to prevent re-absorption, a large Stokes-shift reducing spectral overlap between absorption and emission of the fluorophores is highly favorable. The loss of light can also be reduced by placing mirrors or diffuse reflectors at the bottom and edges of the collector plate. The advantage of LSCs over bare PVCs is that they collect both direct and diffuse sunlight with equal efficiency and deliver concentrated light onto the edge mounted solar cells [4]. In addition, LSCs have the capability to convert a major part of the higher-energy spectrum into photons of a favorable wavelength at which the attached solar cell is the most efficient. LSCs can be fabricated more cheaply than silicon PVCs per square meter. Due to a significant improvement in the photostability of some commercial fluorescent dyes, the LSC concept has re-gained much interest in the last few years. New designs for LSCs, such as uniformly doped sheets with multiple dyes, collector stacks, thin-films doped with one or multiple dyes coated on glass or polymer plates and sol-gel or liquid LSCs, have been reported [3–17].

Instead of organic dyes, inorganic semiconductor nanoparticles (quantum dots, QDs) have been proposed as luminescent

* Corresponding author. Tel.: +49 331 568 1707.

E-mail address: jana.bomm@googlemail.com (J. Bomm).

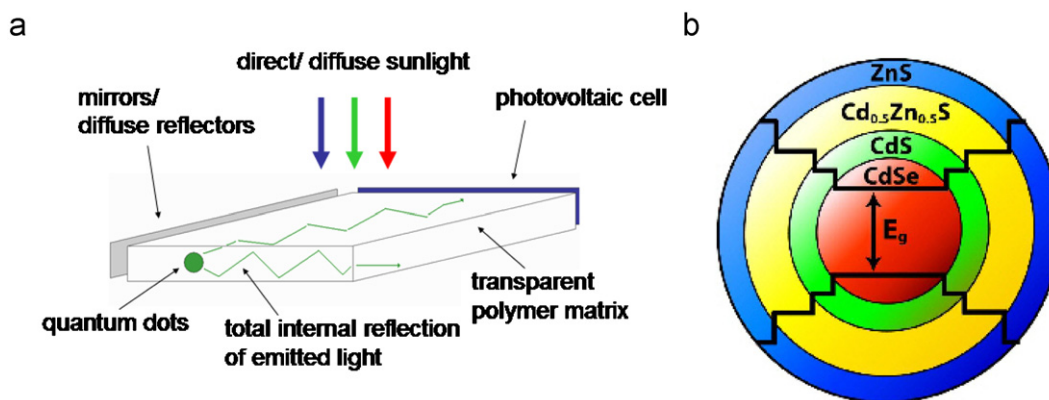


Fig. 1. (a) Schematic illustration of a QD-LSC and (b) a CdSe/CdS/CdZnS/ZnS core/multishell QD.

centers for the LSC. These novel quantum dot luminescent solar concentrators (QD-LSCs) [18–21] have several advantages over organic dye LSCs. QDs are more stable against photodegradation and absorb over a wider spectral range, especially in the UV-region. In addition, the emission wavelength can be readily tuned to a favorable wavelength by changing the QD diameter as a result of quantum confinement effects [22,23]. Last but not the least, the spectral overlap between absorption and emission spectra can be controlled and reduced to a minimum, for example by making use of Type II QDs or PbS QDs [24–27]. In Type II QDs, the band-offset of the materials in e.g. CdTe/CdSe core/shell nanocrystals induce an indirect exciton, which has an emission wavelength that is significantly red-shifted with respect to the direct transitions involved in light absorption. However, the incorporation of inorganic nanoparticles in an organic polymer matrix is regularly accompanied by phase separation and agglomeration of the nanoparticles, which causes turbid nanocomposites and luminescence quenching due to exciton energy transfer [28,29]. Another problem that is typically encountered is chemical attack by radicals during the polymerization process, which also leads to luminescence quenching [29].

Here we report the synthesis and full characterization of QD-LSCs based on CdSe core/multishell QDs incorporated in a dedicated polymer matrix that avoids agglomeration of the nanocrystals. The multiple inorganic shells surrounding the CdSe cores provide sufficient chemical robustness to prevent luminescence quenching due to radicals or photo-oxidation. The composition of the plates is analyzed with transmission electron microscopy (TEM), and the optical properties of the QD-LSCs are analyzed in detail. In addition, the photoaction and quantum efficiency spectra of plates with solar cells attached are presented and analyzed. Furthermore, stability testing under intense light exposure confirms the photostability of the inorganic nanocrystals. The detailed characterization measurements on the LSC plates and test devices were interpreted using a ray-trace model, which was then used to predict the properties of a large area device ($50 \times 50 \text{ cm}^2$). Calculation of the properties of a device of a size that could be used for practical power generation highlights the improvements in the material properties that are required for QD-LSC technology to be commercially exploitable.

2. Material and methods

2.1. Preparation of quantum dot luminescent solar concentrator

CdSe core/multishell QDs were prepared by the SILAR procedure as reported by Xie et al. [30], and described in detail elsewhere [31]. The nanocrystals were purified twice using

hexane and acetone as solvent and nonsolvent, respectively, after which they were dispersed in a small volume of chloroform for further processing. At this stage the QDs were coated by a mixture of the hydrophobic organic ligands oleic acid (OA) and octadecylamine (ODA). The inorganic shells consist of 2 monolayers of CdS, 3 monolayers of $\text{Cd}_{0.5}\text{Zn}_{0.5}\text{S}$ and finally 2 layers of ZnS (see Fig. 1b). In this manner the large lattice mismatch between CdSe and ZnS of 12% is distributed over the intermediate layers, allowing for the growth of a relatively thick inorganic shell around the QD core.

The QDs were dispersed in a monomer mixture of lauryl methacrylate (LMA, Fluka, 98%) with 20 wt% of the cross-linking agent ethylene glycol dimethacrylate (EGDM, Fluka, $\geq 97\%$) and 0.1–0.5 wt% of the liquid UV-initiator Darocure[®] 4265 (Ciba) by ultrasonic treatment. The reaction mixtures were transferred into glass cuvettes and polymerized under a nitrogen atmosphere by illuminating the cuvettes from two sides with UV-A radiation (360 nm) for 15 min. The cuvettes consisted of glass plates with an elastic distance holder between them, which were held together by steel clamps. The polymerized plates were taken out of the cuvettes and illuminated for an additional 2 h to complete curing. The edges of all QD-LSC plates were polished, and a multicrystalline silicon (mc-Si) solar cell was attached to one of the sides using PE 399 KrystalFlex[®] as the bonding agent. KrystalFlex[®] was chosen for its refractive index of 1.49, which is very close to that of the poly(lauryl methacrylate-co-ethylene glycol dimethacrylate) (P(LMA-co-EGDM)) plates, thereby minimizing reflection losses at the interface between the plate and the mc-Si cell.

2.2. Analysis and instrumentation

TEM was performed on thin cryo-cut QD-LSC slices ($755 \text{ nm} \times 565 \text{ nm} \times 65 \text{ nm}$) with a Philips CM200 TEM using a Leica Cryo-Ultramicrotome. Absorption spectra of QD-LSCs were measured using a Perkin Elmer Lambda 950 UV/VIS spectrometer. Emission spectra were recorded using a Perkin Elmer fluorescence spectrometer LS 50 B by exciting the samples at 395 nm. The photoluminescence (PL) quantum yield (QY) was measured at the excitation wavelength of 395 nm (full width at half maximum, FWHM $\sim 5 \text{ nm}$) with a Hamamatsu absolute PL quantum yield measurement system C9920-02. The excitation wavelength is selected from the output of a 150 W xenon lamp by a monochromator. As sample chamber it uses an integrating sphere coupled with a multi-channel CCD spectrometer for signal detection.

For spectral response measurement mirrors were attached to the remaining three edges of the QD-LSC and a diffuse, white

reflector was placed at the bottom of the QD-LSC plate. The external quantum efficiency (EQE) was measured using a spectral response system consisting of a solar simulator, with a 1000 W xenon lamp, and 34 band pass interference filters. Spectral response measurements using a collimated excitation beam was performed by scanning the EQE over a 5×5 grid of points as a function of excitation wavelength using a monochromator with the excitation beam normal to the QD-LSC top surface. Cubic-spline interpolation of the 5×5 grid of points and integration over the surface area of the plate provides the EQE that would be measured if the surface were uniformly illuminated at normal incidence. The overall power conversion efficiency (PCE, η) was calculated by the following equation: $\eta = P_{\text{out}}/P_{\text{in}} = (I_{\text{sc}} V_{\text{oc}} FF) / (P_{\text{lamp}} A)$, where P_{lamp} is the power of the lamp, A is the top surface area of the device, I_{sc} is the short-circuit current, V_{oc} is the open circuit voltage and FF is the fill-factor. The short circuit current (I_{sc}) of the device can be calculated by taking the integral of the overlap between the EQE spectra and the AM1.5G spectrum at 100 mW/cm^2 . The current density on the Si cell (I_{sc} per Si cell area) for the different LSCs was calculated by dividing the total current by the area of the side to which the cell was mounted.

The effect of re-absorption was studied by placing the QD-LSC in a holder and illuminating it such that the path for photons through the plate to the detector (positioned at the side of the plate) was short, medium or long. The QD-LSC was positioned such that the excitation beam (450 W Xe lamp combined with a double grating 0.22 m SPEX monochromator, $\lambda_{\text{ex}} = 406 \text{ nm}$) was normal to the top surface. The QD-LSC of width W (4 cm) and length L (6 cm) was illuminated at $W/2$ and the illumination position along the long axis (L) was adjusted to vary the path length to the detector. A short path length corresponds to excitation near the edge facing the detector, a medium path length corresponds to excitation at $L/2$ and a long path length corresponds to excitation near the edge away from the detector. The emission was measured with a liquid cooled Princeton Instruments CCD camera at one edge of the collector plate (no mirrors). Lifetime measurements were performed using a setup similar to the one described above, replacing the CCD camera by a Hamamatsu photo-multiplier tube (H5738P-01) that is connected to a Time Harp 200 computer card and pulsed PicoQuant laser (2.5 MHz, $\lambda_{\text{ex}} = 406 \text{ nm}$, pulse width = 55 ps) as the excitation source.

Stability tests were performed by measuring the photocurrent of an amorphous Si (a-Si) cell attached to one of the sides of the plates over time. The QD-LSC plates were continuously illuminated by a 1000 W sulfur lamp of which the spectrum is a good match to the solar spectrum particularly in the UV.

3. Results and discussion

3.1. Preparation of quantum dot luminescent solar concentrator

As can be seen in Fig. 1b, the bandgap within the nanocrystal gradually increases from the inside to the outside. This causes an effective scavenging of excitons within the CdSe core, resulting in the required stability against photo-oxidation and chemical attack by radicals. The core/multishell QDs used here have a diameter of $6.7 \pm 0.7 \text{ nm}$ as determined by TEM, and had a quantum yield of 60% in solution. Initial attempts to fabricate optically clear QD/Polystyrene composites were unsuccessful. Dispersing the QDs in styrene lead to agglomeration of QDs and accompanying luminescence quenching. IR-spectra of the agglomerates show that dispersing the QDs in styrene causes a (partial) desorption of the organic ligands from the QD surface, resulting in the observed agglomeration of QDs (see Supplementary data for more details).

Another hydrophobic matrix was chosen to fabricate highly transparent and luminescent QD-LSCs. LMA provides the hydrophobicity required to prevent agglomeration, whereas the cross-linking agent EGDM contributes to the physical strength of the polymer after curing. Transparent and uniform collector plates with excellent surface quality were obtained up to $60 \text{ mm} \times 40 \text{ mm} \times 4.5 \text{ mm}$ in size (see Fig. 2a). The TEM image (Fig. 2b) confirms that the QDs are homogeneously dispersed in the polymer matrix, and only some small agglomerates consisting of a few nanocrystals are observed. We have counted a total number of 272 particles in images from seven different nanocomposite slices. This implies a concentration of $2.33 \mu\text{M}$, which is close to the estimated concentration of $1.64 \mu\text{M}$ in the monomer solution from absorption measurements.

3.2. Optical characterization

Absorption spectra of QD-LSCs with three different concentrations of nanocrystals were measured. The spectra in Fig. 3a show strong absorption at shorter wavelengths, typical for semiconductor nanocrystals and favorable for spectral conversion of sunlight. The first exciton peak of the CdSe cores appears at 606 nm, and in accordance with Beer–Lambert's law the absorption increases linearly with QD concentration. No background absorption is observed at higher wavelengths, which is another indication that the particles are well dispersed in the polymer matrix preventing significant scattering of incoming long wavelength light. After normalization the absorption spectra show exact overlap beyond 450 nm (not shown), which confirms the absence of major scattering by agglomerated nanocrystals. The

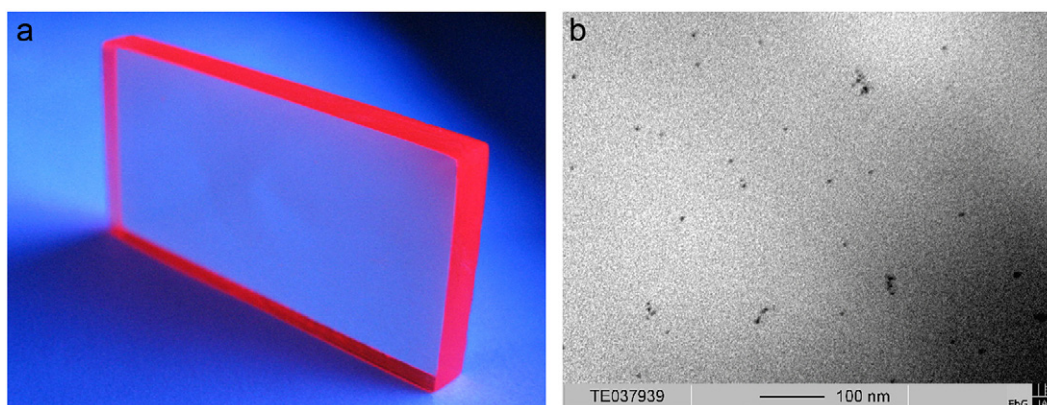


Fig. 2. (a) Photograph of a P(LMA-co-EGDM) plate containing CdSe core/multishell QDs (illuminated by a UV-lamp) illustrating the concentrator effect and (b) TEM image of a QD-LSC/P(LMA-co-EGDM) nanocomposite showing single QDs and a few small QD aggregates.

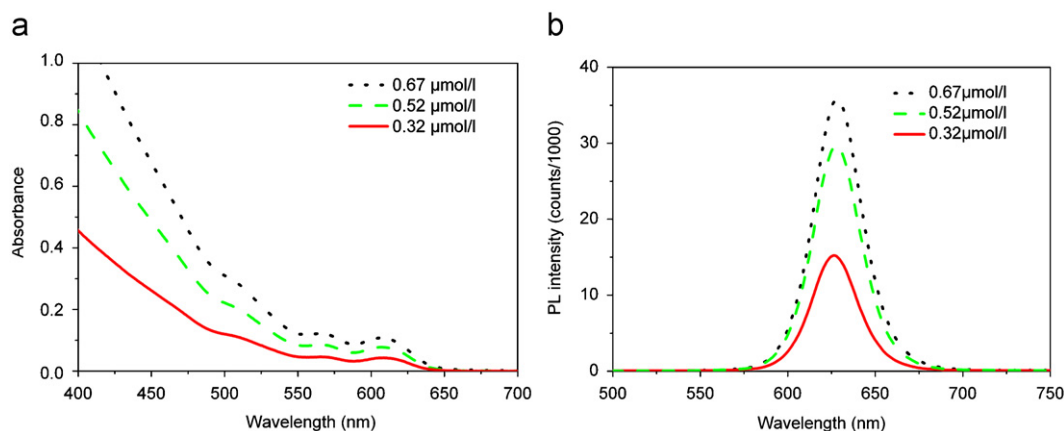


Fig. 3. (a) absorbance and (b) PL spectra of QD-LSCs polymerized from monomer solutions containing 0.1 wt% UV-initiator.

Table 1
Concentrations of QDs and UV-initiator in five different QD-LSCs with corresponding PL quantum yields (QY) and short circuit currents (I_{sc}) of a multicrystalline silicon solar cell attached to one of the QD-LSC sides.

QD-LSC number	Concentration QDs ($\mu\text{mol/l}$)	Concentration UV-initiator (wt%)	QY (%)	I_{sc} total (mA)	Dimensions ($L \times W$, cm) ($h=0.4$ cm)	I_{sc} per Si cell area (mA/cm^2)
1	0.11	0.50	9.0	33.1	5.0×3.8	21.8
2	0.11	0.25	18.1	25.5	3.2×3.3	19.3
3	0.67	0.10	45.4	90.4	4.0×3.8	59.5
4	0.52	0.10	44.2	95.7	5.0×3.1	77.2
5	0.32	0.10	33.3	45.6	4.9×3.8	30.0

photoluminescence (PL) spectra in Fig. 3b show an increase of emission intensity and a slight red-shift of 2 nm for higher QD concentrations.

Instead of thermal polymerization as described by Lee et al. [32] we prefer UV-polymerization because it has been reported that initiator radicals produced from 2,2'-Azobisisobutyronitrile (AIBN) reduces the QY of QDs during the polymerization process [29]. The PL QY of five QD-LSCs with varying QD and UV-initiator concentration was measured (see Table 1). Small cuts ($< 1 \text{ cm}^2$) of the original QD-LSC were used to determine the QY of the QDs in the polymer matrix, to avoid re-absorption losses. A decrease in PL QY in the nanocomposites is observed for higher UV-initiator concentrations (see Table 1), indicating that the UV-initiator also causes PL quenching. We have therefore investigated the minimum amount of UV-initiator that is required in order to obtain stable and fully polymerized plates. Using only 0.1 wt% of initiator, the QD/polymer composites reach quantum yields up to 45%. The relatively small decrease in QY relative to that in dispersion (i.e. from 60% to 45%) may be ascribed to a reduced contact between QDs and UV-initiator radicals during the short UV-polymerization process.

3.3. Spectral response, EQE and PCE

The external quantum efficiency (EQE), also known as incident photon to current efficiency, was measured using a dedicated spectral response system (see Section 2), and the spectra of the various QD-LSCs listed in Table 1 are displayed in Fig. 4. It can be observed that there is a clear contribution from the QDs to the photocurrent at wavelengths less than 650 nm where the QDs absorb, but a large contribution from incident light reaching the mc-Si cell was measured at longer wavelengths as well. There are two mechanisms in the QD-LSC that contribute to this response to unabsorbed incident light. The first is scattering; although the absorption spectra do not show evidence of significant scattering

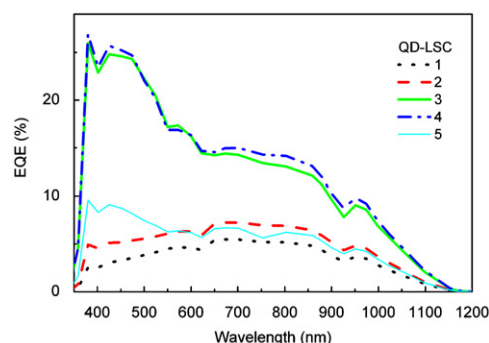


Fig. 4. EQE spectra of the five QD-LSCs (numbers corresponding to Table 1) doped with CdSe core/multishell-QDs measured using the spectral response system (see main text).

by agglomerated nanocrystals, surface irregularities and density variations in the polymer host matrix will undoubtedly cause some small scattering effects. Secondly, even if the incident light were perfectly collimated, the diffuse back surface reflector will reflect light at wide angles which, near the edge of the QD-LSC, may be refracted back into the device such that it reaches the cell. The contribution of the QDs to the EQE below 650 nm is only significant for those LSCs that have a relatively high QY of the QDs (QD-LSC 3 and 4), whereas the contribution of the QDs is minimal (QD-LSC 5) or even negative for lower QYs (QD-LSC 1 and 2). This emphasizes the importance of a high QY of the fluorophores to overcome losses due to re-absorption process, as will be discussed further below.

The total short circuit currents and the short circuit currents per Si cell area for the different QD-LSCs are given in Table 1. Compared to the bare mc-Si cell ($5 \times 0.5 \text{ cm}^2$), which generates $40.3 \text{ mA}/\text{cm}^2$ upon direct illumination, QD-LSCs 3 and 4 exhibit current density increases of 48% and 91%. Although these two QD-LSCs had nearly the same

surface area ($\sim 15 \text{ cm}^2$) and measured QYs, QD-LSC 3 generates a lower photocurrent density than QD-LSC 4. This is explained by the higher QD-concentration in QD-LSC 4, which leads to stronger re-absorption losses. It was found that smaller pieces of the QD-LSCs gave higher photocurrents, which also indicates that re-absorption by the QDs and absorption by the polymer matrix plays an important role in larger QD-LSCs. With a lamp power of 0.1 W/cm^2 (1000 W/m^2), a top surface area of 15.4 cm^2 ($4.95 \text{ cm} \times 3.1 \text{ cm} \times 0.4 \text{ cm}$), an I_{sc} of 95.7 mA (77.2 mA/cm^2), a V_{oc} of 0.6 V and a fill-factor of 0.76 the experimentally determined PCE for QD-LSC 4 is 2.8% .

In order to interpret the results with a model for the QD-LSC the angular distribution of the incident light must be known. In addition, it is important to be able to discriminate between the contributions of QD-fluorescence and scattered light to the measured EQE. It was therefore decided to investigate the spectral response of QD-LSC 3 in detail using a collimated excitation beam (see Section 2 for details). For these measurements the mc-Si cell was replaced by a GaAs cell (again bonded with KrystalFlex) and two configurations were studied. Firstly the EQE was measured without reflectors on the edges and with a black cloth (low reflectivity) under the bottom surface of the QD-LSC and secondly the configuration with mirror foil edge reflectors and a diffuse, white polytetrafluoroethylene (PTFE) bottom reflector was studied. The interpolated and integrated results, together with the predictions of a ray-trace model, are shown in Fig. 5.

As can be seen in Fig. 5, using this collimated excitation beam results in a much smaller contribution from unabsorbed incident light at wavelengths beyond 650 nm compared to the results in Fig. 4. As expected this contribution to the EQE beyond 650 nm is the smallest for the sample without back and side reflectors (Fig. 5a). It is further noted that the EQE measurements show an excellent agreement with the absorption spectra displayed in Fig. 3. The experimental results in Fig. 5 can largely be explained using the model for the QD-LSC. The ray-trace model [33–35] uses geometrical optics to trace the path of individual photons through the QD-LSC during which Monte Carlo methods are used to determine the outcome of events by mapping a random number generator onto the appropriate distributions. Intersections with surfaces are computed and experimentally measured absorption spectra are substituted into the Beer–Lambert Law to determine the free path of a photon in a given direction. At each surface the reflection coefficient is calculated from the Fresnel equations and the measured reflectivity of any reflectors is used where appropriate. In the case of transmission through a surface Snell's law is applied to determine

the refraction. A photon can be absorbed by the host polymer matrix or by the QDs and is re-emitted depending on the QY. The wavelength of a re-emitted photon is generated based on an experimental emission spectrum measured under conditions that minimize the red-shift due to re-absorption. The EQE of the devices when fully illuminated were then calculated using the measured EQE of the GaAs cell used.

As can be seen in Fig. 5a the response of the device to unabsorbed incident light at wavelengths beyond 650 nm is reproduced exactly by the model when no reflectors are used. This configuration minimizes the average path length through the device and the measured reflectivity of the black cloth is responsible for the increase seen between 700 and 900 nm with the sharp cut off at just below 900 nm due to the sharp fall in cell EQE approaching the band-gap of GaAs. However, as can be seen in Fig. 5b, when reflectors are used, thereby maximizing the average path length in the device, there is no longer such an exact correspondence between the experimental and simulation results at wavelengths beyond 650 nm . This is most likely due to the surface and host matrix scattering effects described above, that are not included in the model, which are more evident here owing to the longer path lengths. The reason for the increasing discrepancy at short wavelengths between the model and experiment, seen for both configurations, is less easy to pinpoint. Firstly the cell response may be non-linear at the low monochromator light intensities used in this work. Secondly the PL QY, which is assumed to be constant over the wavelength range of interest in the simulations, may vary with wavelength. Finally, the filter and grating combination used in the monochromator may not be as effective at providing monochromatic light at short wavelengths and it is possible that an increasing degree of white light leaking through from the lamp is responsible for the discrepancy. Further analysis to identify the reason is beyond the scope of this work and will be the subject of further study together with detailed measurements of the scattering properties of QD-LSC plates.

The power conversion efficiencies of a $50 \times 50 \text{ cm}^2$ QD-LSC, which could be used for practical collection purposes, was estimated using the ray-trace model with different types of solar cells. The PCE was estimated using the ray-trace model with different types of solar cells (InGaP, GaAs and mc-Si) attached to all four edges. The properties of QD-LSC 3 were used as input for these simulations except that the QY was increased to 90% . The current practically achievable QY for QDs is $\sim 85\%$ [36] and 90% therefore represents a target value that could be achieved in the near term given appropriate development. A $50 \times 50 \text{ cm}^2$ square device was simulated under uniform illumination by AM1.5G at

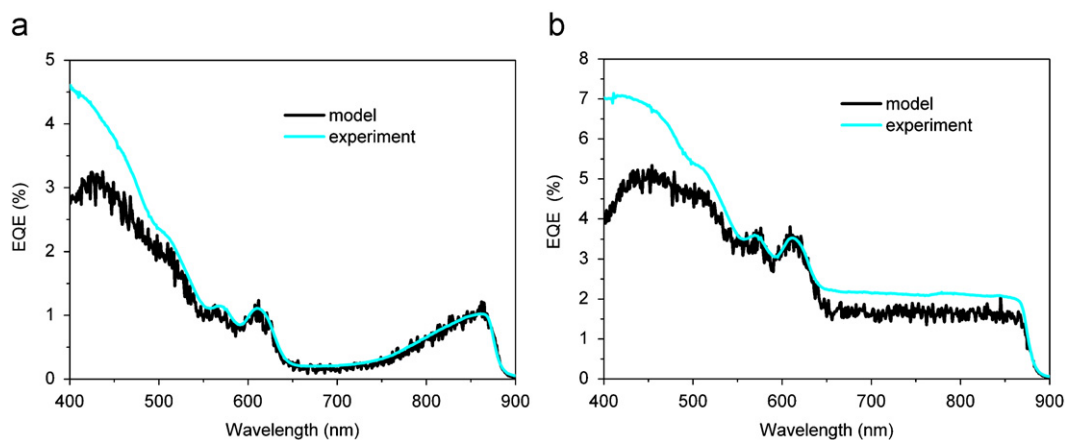


Fig. 5. Experimental and simulated EQE spectra of QD-LSC 3 in two contrasting configurations: (a) with no reflectors and a black cloth background and (b) with mirror foil edge reflectors and diffuse back reflector.

normal incidence with a diffuse back reflector using the EQE and dark current measurements of test cells available at our laboratories. To calculate the PCEs it was assumed that the I - V response of the device can be approximated by the subtraction of the dark current from the short circuit current (commonly termed additivity or superposition).

The predicted PCEs for attached InGaP, GaAs and mc-Si cells are 0.67%, 0.84% and 0.50%, respectively. The value for attached InGaP cells is lower than that for GaAs because despite its higher band-gap giving a higher output voltage the EQE of the InGaP cells is lower than that for the GaAs cells within the wavelength range of the emission thus limiting the short-circuit current. GaAs cells therefore represent an optimum for this device but would be prohibitively expensive in practice. An economic but lower efficiency (owing to the lower band-gap) configuration is that with attached mc-Si cells. However, the PCE of 0.5% is still too low for commercial generation purposes. The QDs used in this work only absorb 31% of the AM1.5G spectrum between 300 and 1100 nm that is available to Si cells. To improve the PCE broader absorption up to the near IR would be required in addition to much lower re-absorption losses. Broader absorption could be achieved either by using larger QDs or by changing material system and our analysis shows that if re-absorption losses were minimized the device efficiency would be approximately doubled. Therefore broader absorption and emission at wavelengths near the band-gap of Si, together with reduced re-absorption losses, could therefore lead to practical sized devices with PCEs nearing 5%.

3.4. Re-absorption and lifetime measurements

To study the effect of re-absorption in more detail, QD-LSC 3 was illuminated such that the path for photons through the plate to the detector was either short, medium or long. The corresponding normalized experimental emission spectra shown in Fig. 6a clearly show an increasing red-shift (up to 10 nm) with increasing photon path length. This, together with the reduction in intensity also seen with increasing path length (not shown), can be readily explained by the re-absorption process, since it introduces a further chance of exciton trapping (reducing emission intensity), and inherently causes a red-shift owing to the Stokes-shift of the QDs. The ray-trace model used allows position dependent illumination and was applied to simulate the emission spectra from the edge facing the detector for the different path lengths by logging the number and wavelengths of all photons

exiting that face. The results are shown in Fig. 6b and the increasing red-shift and narrowing of the spectra at short wavelengths are reproduced exactly, increasing our confidence in using the ray-trace model to predict the properties of larger devices. Although the simulated results also showed a decrease in intensity for longer path lengths the results in Fig. 6 are normalized because the experimental collection optics cannot be easily reproduced by the model. The modeling results confirm that re-absorption is the cause of the increasing red-shift seen for longer path lengths.

We have also performed lifetime measurements. The decay curves for QD-LSC 3 are nearly single exponential (see Fig. 7a), in accordance with the relatively high QY of the QDs. An average exciton lifetime (τ) of 19 ns is found in the case of the short photon path length, when fitted to a single exponential function, see Fig. 5 of the supporting information. A longer path length for photons traveling through the plate increases the chances of re-absorption. For each re-absorption event, the photon is delayed by on average 19 ns (τ). This effect can be seen in Fig. 7a, but appears to be weak at first sight. However, when the difference between the two decay curves is plotted, it can clearly be seen that there is an increasing delay for the first 20 ns, after which it decays to zero (Fig. 7b). This indicates that photons, which have the longer path length are on average re-absorbed once. This is confirmed using the ray-trace model and Fig. 7b shows excellent agreement between the simulated and experimental difference spectra.

In Fig. 7b the instrument delay time of 25 ns that can be seen in Fig. 7a has been subtracted in order to compare the modeling and experimental results. To simulate the lifetime measurement data using the ray-trace model, it was assumed that the underlying lifetime distribution (with no influence from re-absorption, which is always contributing to the experimental measurements to some extent) was single exponential, varying as $\exp(0.077 t)$ where t is the time in ns (i.e. an average excitation lifetime of 13 ns). This choice, that gave the best agreement between the simulations and experiment, was informed by the fact that the experimental curve for the short path length was in fact better described by a bi-exponential fit resulting in fast and slow components of 13 and 30 ns, respectively (see Fig. 5 of the Supporting information). In the simulations the number of re-absorptions undergone by all photons exiting the edge facing the detector was logged for the different excitation positions. In order to build the simulated lifetime distributions lifetimes for the initial and any subsequent emission events were assigned for each logged photon by mapping the underlying lifetime

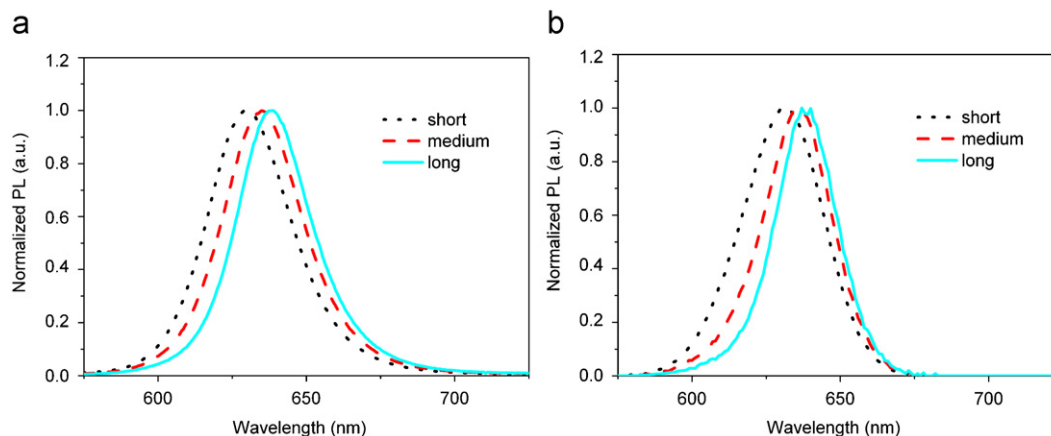


Fig. 6. (a) Experimental and (b) simulated normalized emission spectra from the edge facing the detector for the spot excitation positions giving short, medium and long path lengths to the detector.

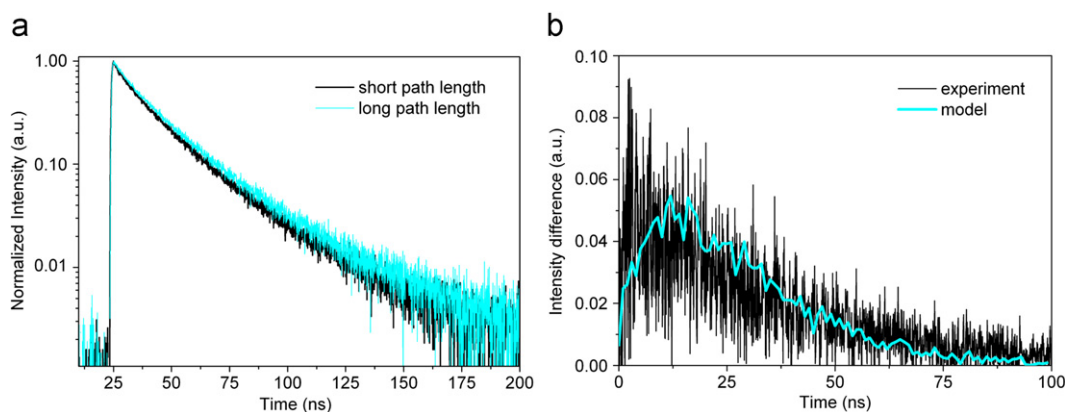


Fig. 7. (a) Decay curves of QD-LSC number 3 measured at the emission peak (634 nm) for the short (black line) and long (red line) photon path lengths and (b) experimental and simulated difference spectra of the two decay curves. (For interpretation of the references to color in this figure legend, the reader is referred to the web version of this article.)

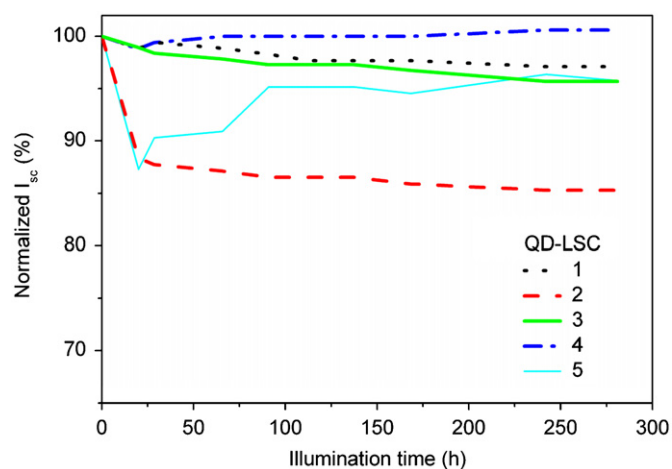


Fig. 8. Short circuit current of various QD-LSCs as a function of illumination time using a 1000 W sulfur lamp as light source.

distribution to a probability density that was sampled as usual by a random number. Although the choice of a single exponential may not be an absolutely accurate representation of the underlying lifetime distribution, the excellent agreement between the simulations and the experiments shows that the difference between the measurements with short and long path lengths to the detector is predominantly due to re-absorption and further shows that the ray-trace model accurately deals with this mechanism. It should be noted that the chance of detecting photons that are re-absorbed more than once is relatively low, due to the QY of 45%.

3.5. Stability testing

Despite recent encouraging results [35], the stability of in-solated organic dye doped luminescent concentrators is known to be a particular problem. Therefore accelerated stability tests were performed. The photocurrents in Fig. 8 were normalized to the values obtained before illumination. After an illumination time of 280 h, which is equivalent to about 3 months of outdoor exposure, the short circuit current is on average reduced to 96% of the initial photocurrent. This confirms the photostability of the inorganic nanocrystals under relatively severe conditions. The origins of the relatively large decrease seen for QD-LSC number 5 to 85% of the initial value and the initial decrease followed by a recovery seen for QD-LSC 1 are unclear. Further accelerated aging experiments will be performed to investigate the stability of the

QD-LSCs over the timescales that would be required for commercial exploitation (i.e. 20–30 years of outdoors exposure).

4. Conclusions

In summary, the detailed analysis of QD-based LSCs reported here reveals both the strong and the weak aspects of this concept. On the one hand, it is shown that transparent and fluorescent plates containing well-dispersed QDs can be fabricated, and that the inorganic fluorophores are stable under intense illumination over long periods of time. With a final QY of the QDs in the polymer matrix of 45% an overall PCE of 2.8% was obtained, albeit for relatively small samples (15 cm²). On the other hand, ray-trace modeling shows that even if the QY of the QDs is assumed to be 90%, an overall PCE of only 0.5% is obtained for a QD-LSC with attached Si cells with 50 cm × 50 cm dimensions. The modeling shows that for the QD-LSC concept to be commercially viable, the absorbance of QDs should be higher and extend further into the NIR, and re-absorption losses should be drastically reduced, for example by using QDs that exhibit a large Stokes-shift. In that respect, the properties of Type II QDs [24–26] or small PbS QDs [27], which both exhibit NIR emission combined with a large Stokes-shift is especially encouraging. Using such materials, practical devices could theoretically achieve PCEs up to 5%.

Acknowledgments

Financial support from the European Union Framework 6 Integrated Project “FULLSPECTRUM” (SES6-CT-2003-502620) is gratefully acknowledged. Manfred Pinnow and Marion Schlawne of Fraunhofer-IAP are acknowledged for their help in the TEM investigation.

Appendix A. Supplementary material

Supplementary data associated with this article can be found in the online version at doi:10.1016/j.solmat.2011.02.027.

References

- [1] W.H. Weber, J. Lambe, Luminescent greenhouse collector for solar radiation, *Appl. Opt.* 15 (1976) 2299–2300.
- [2] A. Goetzberger, W. Greubel, Solar energy conversion with fluorescent collectors, *Appl. Phys.* 14 (1977) 123–139.

- [3] S.T. Bailey, G.E. Lokey, M.S. Hanes, J.D.M. Shearer, J.B. McLafferty, G.T. Beaumont, T.T. Baseler, J.M. Layhue, D.R. Broussard, Y.-Z. Zhang, B.P. Wittmershaus, Optimized excitation energy transfer in a three-dye luminescent solar concentrator, *Sol. Energy Mater. Sol. Cells* 91 (2007) 67–75.
- [4] W. Stahl, A. Zastrow, Fluoreszenzkollektoren, *Physik in unserer Zeit* 6 (1985) 167–179.
- [5] A.F. Mansour, H.M.A. Killa, S. Abd El-Wanees, M.Y. El-Sayed, Laser dyes doped with poly(ST-Co-MMA) as fluorescent solar collectors and their field performance, *Polym. Test.* 24 (2005) 519–525.
- [6] R. Reisfeld, D. Shamrakov, C. Joergensen, Photostable Solar Concentrators based on fluorescent glass films, *Sol. Energy Mater. Sol. Cells* 33 (1994) 417–427.
- [7] R. Reisfeld, Prospects of sol-gel technology towards luminescent materials, *Opt. Mater.* 16 (2001) 1–7.
- [8] V.V. Popov, V.N. Yakimenko, State of the art of prospects for investigations of luminescent solar concentrators, *J. Appl. Spectrosc.* 62 (1995) 573–577.
- [9] A.F. Mansour, Outdoor testing of luminescent solar concentrators in a liquid polymer and bulk plate of PMMA, *Polym. Test.* 17 (1998) 153–162.
- [10] A.F. Mansour, M.G. El-Shaarawy, S.M. El-Basir, M.K. El-Mansy, M.A. Hammam, A qualitative study and field performance for a fluorescent solar collector, *Polym. Test.* 21 (2002) 277–281.
- [11] P.D. Swift, G.B. Smith, Color considerations in fluorescent solar concentrator stacks, *Appl. Opt.* 42 (2003) 5112–5117.
- [12] A.A. Earp, G.B. Smith, J. Franklin, P. Swift, Optimisation of a three-colour luminescent solar concentrator daylighting system, *Sol. Energy Mater. Sol. Cells* 84 (2004) 411–426.
- [13] A.A. Earp, G.B. Smith, P.D. Swift, J. Franklin, Maximising the light output of a luminescent solar concentrator, *Sol. Energy Mater. Sol. Cells* 76 (2004) 655–667.
- [14] B.A. Swartz, T. Cole, A.H. Zewail, Photon trapping and energy transfer in multiple-dye plastic matrices: an efficient solar-energy concentrator, *Opt. Lett.* 1 (1977) 73–75.
- [15] A.M. Hermann, Luminescent solar concentrators—a review, *Sol. Energy* 29 (1982) 323–329.
- [16] V. Sholin, J.D. Olson, S.A. Carter, Semiconducting polymers and quantum dots in luminescent solar concentrators for solar energy harvesting, *J. Appl. Phys.* 101 (2007) 1231141–1231149.
- [17] L.H. Slooff, E.E. Bende, A.R. Burgers, T. Budel, M. Pravettoni, R.P. Kenny, E.D. Dunlop, A. Büchtemann, A luminescent solar concentrator with 7.1% power conversion efficiency, *Phys. Status Solidi Rapid Res. Lett.* 2 (2008), pp. 257–259.
- [18] A.J. Chatten, K.W.J. Barnham, B.F. Buxton, N.J. Ekins-Daukes, M.A. Malik, A new approach to modelling quantum dot concentrators, *Sol. Energy Mater. Sol. Cells* 75 (2004) 363–371.
- [19] A.J. Chatten, K.W.J. Barnham, B.F. Buxton, N.J. Ekins-Daukes, M.A. Malik, Quantum dot solar concentrators, *Semiconductors* 38 (2004) 909–917.
- [20] K.W.J. Barnham, J.L. Marques, J. Hassard, P. O'Brien, Quantum-dot concentrator and thermodynamic model for the global redshift, *Appl. Phys. Lett.* 76 (2000) 1194–1197.
- [21] A.J. Chatten, R. Bose, D.J. Farrell, Y. Xiao, N.L.A. Chan, L. Manna, A. Büchtemann, J. Quilitz, M.G. Debije, K.W.J. Barnham, Luminescent solar concentrators, in: L. Tsakalacos (Ed.), *Nanotechnology for Photovoltaics*, CRC Press Taylor & Francis Group, Boca Raton, , 2010, pp. 330–331.
- [22] R.A. Bley, S.M. Kauzlarich, Synthesis of silicon nanoclusters, in: J.H. Fendler (Ed.), *Nanoparticles and Nanostructured Films*, Wiley-VCH Verlag, Weinheim, , 1998, pp. 101–103.
- [23] C.B. Murray, D.J. Norris, M.G. Bawendi, Synthesis and characterization of nearly monodisperse CdE ($E = \text{sulfur, selenium, tellurium}$) semiconductor nanocrystallites, *J. Am. Chem. Soc.* 115 (1993) 8706–8715.
- [24] R. Xie, X. Zhong, J. Li, T. Basché, Synthesis, characterization, and spectroscopy of type-II core/shell semiconductor nanocrystals with ZnTe cores, *Adv. Mater.* 17 (2005) 2741–2745.
- [25] S. Kim, B. Fisher, H.-J. Eisler, M.G. Bawendi, Type-II quantum dots: CdTe/CdSe(core/shell) and CdSe/ZnTe (core/shell) heterostructures, *J. Am. Chem. Soc.* 125 (2003) 11466–11467.
- [26] P.T.K. Chin, C. de Mello Donega, S.S. van Bavel, S.C.J. Meskers, N.A.J.M. Sommerdijk, R.A.J. Janssen, Highly luminescent CdTe/CdSe colloidal heteronanostructures with temperature-dependent emission color, *J. Am. Chem. Soc.* 129 (2007) 14880–14886.
- [27] G.V. Shcherbatyuk, R.H. Inman, C. Wang, R. Winston, S. Ghosh, Viability of using near infrared PbS quantum dots as active materials in luminescent solar concentrators, *Appl. Phys. Lett.* 96 (2010) 191901–191904.
- [28] R. Koole, P. Liljeroth, C. de Mello Donega, D. Vanmaekelbergh, A. Meijerink, Electronic Coupling and exciton energy transfer in CdTe quantum-dot molecules, *J. Am. Chem. Soc.* 128 (2006) 10436–10441.
- [29] C. Woelfle, R.O. Claus, Transparent and flexible quantum dot-polymer composites using an ionic liquid as compatible polymerization medium, *Nanotechnology* 18 (2007) 0254021–0254029.
- [30] R. Xie, U. Kolb, J. Li, T. Basché, A. Mews, Synthesis and characterization of highly luminescent CdSe-Core CdS/Zn_{0.5}Cd_{0.5}S/ZnS multishell nanocrystals, *J. Am. Chem. Soc.* 127 (2005) 7480–7488.
- [31] R. Koole, M.M. van Schooneveld, J. Hilhorst, C. de Mello Donega, D.C. 't Hart, A. van Blaaderen, D. Vanmaekelbergh, A. Meijerink, The incorporation mechanism of hydrophobic quantum dots in silica spheres by a reverse microemulsion method, *Chem. Mater.* 20 (2008) 2503–2512.
- [32] J. Lee, V.C. Sundar, J.R. Heine, M.G. Bawendi, K.F. Jensen, Full color emission from II–VI semiconductor quantum dot-polymer composites, *Adv. Mater.* 12 (2000) 1102–1105.
- [33] R. Bose, D.J. Farrell, A.J. Chatten, M. Pravettoni, A. Büchtemann, J. Quilitz, A. Fiore, L. Manna, K.W.J. Barnham, Luminescent solar concentrators: nanorods and raytrace modeling, in: *Proceedings of the 33rd IEEE Photovoltaics Specialist Conference*, San Diego, USA, 2008, 24–28.
- [34] A.R. Burgers, L.H. Slooff, R. Kinderman, J.A.M. van Roosmalen, Modeling of luminescent concentrators by ray-tracing, in: *Proceedings of the Twentieth European Photovoltaic Solar Energy Conference Munich*, Germany, 2005, pp. 394–397.
- [35] W.G.J.H.M. van Sark, K.W.J. Barnham, L.H. Slooff, A.J. Chatten, A. Büchtemann, A. Meyer, S.J. McCormack, R. Koole, D.J. Farrell, R. Bose, E. Bende, A.R. Burgers, T. Budel, J. Quilitz, M. Kennedy, T. Meyer, S.H. Wadman, G. van Klink, G. van Koten, A. Meijerink, D. Vanmaekelbergh, Luminescent solar concentrators—a review of recent results, *Opt. Express* 16 (2008) 21773–21792.
- [36] P. Reiss, J. Bleuse, A. Pron, Highly luminescent CdSe/ZnSe core/shell nanocrystals of low size dispersion, *Nano Lett.* 2 (2002) 781–784.